Virtual Synchronous Machine Control of VSC HVDC for Power System Oscillation Damping

Javier Roldán-Pérez*, Jon Are Suul†, Salvatore D'Arco†, Alberto Rodríguez-Cabero*, and Milan Prodanovic*
*IMDEA Energy Institute, Madrid, Spain. †SINTEF Energy Research, Trondheim, Norway.
javier.roldan@imdea.org, {jon.a.suul, salvatore.darco}@sintef.no, {alberto.rodriguez, milan.prodanovic}@imdea.org

***Abstract*—Two different methods for implementing inertial damping on a Virtual Synchronous Machine (VSM) and their potential for attenuating power system oscillations when utilized in a VSC HVDC terminal are investigated in this paper. As a reference case, the VSM is considered with only a frequency droop providing damping in the virtual swing equation. Then, the effect of damping based on high-pass filtering of the virtual speed is compared to damping based on high-pass filtering of the measured grid frequency. A simplified model of a power system with two equivalent generators and a VSC HVDC terminal is introduced as a case study. Analysis of the small-signal dynamics indicates that damping based on the VSM speed has limited influence on the power system oscillations, while improved attenuation can be obtained by introducing damping based on the locally measured grid frequency. The presented analysis and the operation of the proposed VSM-based damping strategy is validated by numerical simulation of a 150 MVA VSM controlled VSC HVDC terminal connected to a dynamic model of the assumed grid configuration.**

***Index Terms*—Power System Oscillation Damping, Virtual Inertia, Virtual Synchronous Machine, VSC-HVDC.**

I. Introduction

HVDC transmission systems have for long time been utilised to damp oscillations in power systems by introducing additional damping controllers. The first examples of such auxiliary control functions for damping low frequency oscillations were implemented with traditional thyristor-based HVDC terminals [1–3]. However, modern Voltage Source Converter (VSC) technology provides faster control response and decoupled control of active and reactive power. Thus, VSC HVDC terminals can provide power oscillation damping as well as additional ancillary services, and can allow for fast primary frequency control influencing the equivalent inertial response of the ac power system [4–6]. The fast response can also enable VSC HVDC converter stations to provide virtual inertia support to the power system by emulating the inertial response of synchronous machines [7–9].

With increasing share of converter interfaced generation and corresponding decommissioning of traditional power plants, the potential for providing virtual inertia from HVDC converter stations is expected to become increasingly important. Such virtual inertia control can generally be implemented by two approaches [10]: i) *Frequency-derivative-based Inertia Emulation* (df/dt-IE), where the power response that a synchronous machine would provide is calculated from the measured grid frequency and added to the power reference of a conventional control system. ii) *Virtual Synchronous Machines* (VSMs), where the control system relies on an internal simulation of a virtual swing equation with its corresponding power-balance-based grid synchronization mechanism. Utilization of df/dt-IE control allows for inertia emulation as an added feature of a conventional control system based on grid synchronisation and frequency measurement by a Phase Locked Loop (PLL), but relies on a relatively strong grid. However, VSMs can operate in islanded conditions and inertia-less power systems, as well as under strong grid conditions.

Because of the operational flexibility offered by VSM-based control strategies, a wide range of implementations and applications have been proposed [8, 10–14]. Furthermore, auxiliary functions for supporting the power system operation can be integrated in the VSM control framework as discussed in [15–18]. Several recent studies have also analysed how VSM-based control schemes can be utilised to damp local oscillations in small-scale power systems [15, 16, 19, 20]. However, less attention has been directed towards the application of VSM-based control for damping of low frequency oscillations. Thus, only a few publications have addressed how VSMs can be utilized to influence oscillations originating from existing synchronous machines in a large-scale power system [21, 22].

In this paper, the utilisation of a VSM for damping of power system oscillations based only on local measurements is investigated. For this purpose, a simplified model of a power system with two equivalent generators is introduced. This

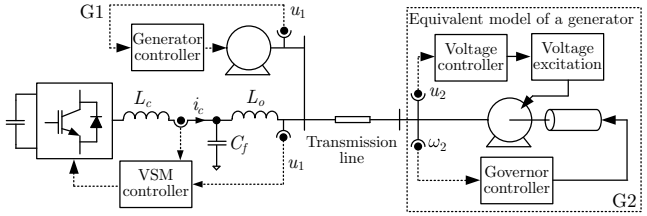

Fig. 1. Power system including two equivalent synchronous generators connected by a transmission line and a HVDC terminal controlled as a VSM.

The work of IMDEA Energy Institute in this paper received financial support from the Community of Madrid Government, Spain, through the research project PRICAM (S2013/ICE-2933), and from the mobility program Jose Castillejo (CAS17/00386) funded by the Spanish Government. The work of SINTEF Energy Research was supported by the project HVDC Inertia Provision (HVDC Pro), financed by the ENERGIX program of the Research Council of Norway (project number 268053/E20) and the industry partners; Statnett, Equinor, RTE and ELIA.

This is the accepted version of a paper published in 44th Annual Conference of the IEEE Industrial Electronics Society (IECON2018)
DOI: 10.1109/IECON.2018.8591097

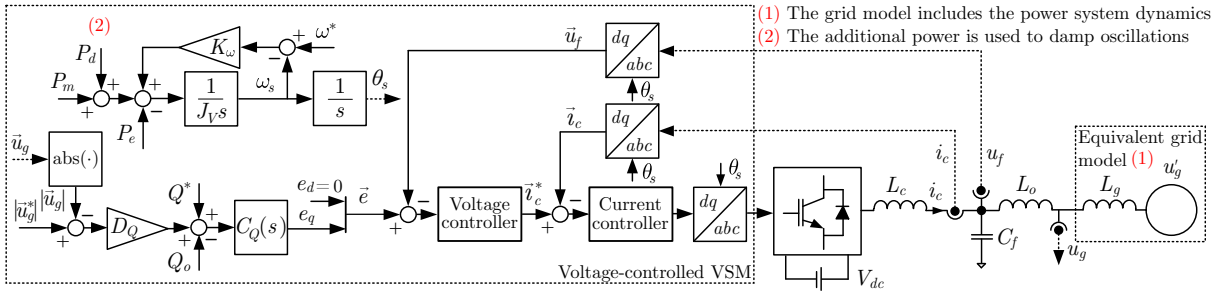

Fig. 2. Electrical and control system overview for the VSM connected to the power system.

model allows for small-signal analysis of how the control of a VSM will influence the oscillations in the power system. Then, two different implementations of the internal damping of the VSM are presented and a parametric analysis of the simplified system model is conducted to study the impact on the power system oscillations. By this analysis, it is demonstrated that implementation of the VSM damping based only on the local virtual speed has limited capability for damping the power system oscillations. Instead, additional damping based on the measured grid frequency can help to attenuate the oscillations between the two generators. The assumed damping based on the measured grid frequency has the same form as commonly applied for df/dt-IE. Thus, the obtained results indicate that improved damping of power system oscillations based only on local measurements can be achieved by introducing an additional df/dt-based term in the power balance of the virtual swing equation of a VSM. The obtained results are verified by time domain simulation of the studied system configuration.

II. System Overview and Modelling

This section provides an overview of the system configuration and the VSM scheme assumed in this paper. Moreover, the applied mathematical models will be presented.

A. Reference power system configuration

This paper will consider the power system configuration presented in Fig. 1, represented by two equivalent synchronous generators, referred to as G1 and G2, connected via a transmission line. The two generators are locally controlled with a conventional governor to regulate their speed and an exciter to control their rotor field. In Fig. 1 these regulators are displayed separately for G2 and aggregated in the block labelled "Generator Controller" for G1. The transmission line is modelled as a constant impedance. This power system has been configured to exhibit oscillations between the two equivalent generators.

As shown in Fig. 1, a VSC-HVDC terminal is connected in parallel to G1. The HVDC terminal is assumed to be a 2 level VSC with an *LCL* ac filter. The dynamics on the dc side of the HVDC terminal are neglected and the dc link is modelled as a constant dc voltage source. The HVDC terminal is assumed to be controlled as a VSM. The main function of the HVDC terminal is import or export of power, and the VSM-based control is introduced for providing inertial support to the ac system. However, this paper will explore the capabilities of the VSM-controlled HVDC terminal to damp the oscillations between the generators.

B. Virtual Synchronous Machine Overview

The circuit configuration of the HVDC terminal and the VSM control scheme are displayed in Fig. 2. The converter-side series inductance and resistance in the *LCL* filter are denoted as L_c and R_c while the grid-side series inductance and resistance are denoted as L_o and R_o. The filter capacitance is indicated as C_f. The grid voltage is denoted as u_g, while i_c is the converter-side current, and i_o is the current injected to the grid. The control of the VSM is based on the scheme presented in [11] with an inner current control loop cascaded with an external voltage control. The two controllers are implemented in a synchronous reference frame (SRF). Space vectors in the SRF are noted with an arrow over the variable name, while dq axis components are noted in the subscript (e.g. $\vec{u}_g = u_{g,d} + ju_{q,d}$). The converter-side current is controlled with a space-vector-based PI controller applied to i_c, while the capacitor voltage u_f is controlled by another PI controller.

The phase angle orientation of the control system is given by an inertia model. The inertia model of the VSM is based on a classical swing equation representation of a synchronous machine and modelled in the Laplace domain as [10]:

$$J_V \cdot s \cdot \omega_s = P_m - P_e - P_d - K_\omega \tag{1}$$

where J_V is the virtual inertia, K_ω is the droop coefficient, ω_s is the angular frequency of the VSM and ω_s^* is its reference value, P_e is the electrical output power, and P_m is the mechanical power. The variable P_d represents the damping of the swing equation, including the additional power that is used in this paper to damp the power system oscillations. This term will be further discussed in Section III.

The phase angle used for Park transformations in the control system is obtained by integrating the generator frequency:

$$\theta_s = 1/s \cdot \omega_s \tag{2}$$

The variable e_q represents the amplitude of the voltage reference for the voltage controller and is used to control the reactive power:

$$e_q = K_Q \cdot (Q^* - Q - Q_D) \cdot 1/s, \tag{3}$$

This is the accepted version of a paper published in 44th Annual Conference of the IEEE Industrial Electronics Society (IECON2018)
DOI: 10.1109/IECON.2018.8591097

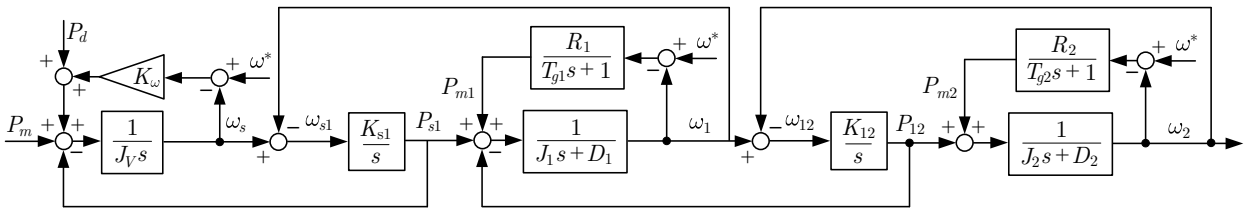

Fig. 3. Mathematical model of the power system with a VSM integrated

where Q_D is the reactive power difference provided by the voltage droop, Q^* is the reference value, Q is the reactive power injected to the grid, and K_Q is the controller gain. The voltage droop in the reactive power reference is calculated as:

$$Q_D = D_Q \cdot (|\vec{u}_g^*| - |\vec{u}_g|), \tag{4}$$

where D_Q is the droop coefficient and $|\vec{u}_g^*|$ is the grid voltage set point.

C. Power system modelling

The mathematical model of the electrical grid presented in Section II-A can be expressed in terms of transfer functions. The synchronous generators are represented with a first order transfer function representing their swing equations. For G1, J_1 and D_1 indicate the inertia and the damping factor. The mechanical power is denoted as P_{m1} while the electromechanical power is indicated as P_{e1}. Thus, the generator angular frequency can be obtained as:

$$\omega_1(s) = 1/(J_1 s + D_1) \cdot (P_{m1}(s) - P_{e1}(s)). \tag{5}$$

The phase of the generator voltage θ_1 can be obtained by integration of the angular frequency as:

$$\theta_1(s) = 1/s \cdot \omega_1(s). \tag{6}$$

The output power of the generation units is controlled via a governor represented as a first order transfer function with a time constant T_{g1} and a droop coefficient R_1. The mechanical power for G1 is calculated as:

$$P_{m1}(s) = (R_1/(T_{g1}s + 1))(\omega^*(s) - \omega_1(s)), \tag{7}$$

where the superscript "*" represents the set-point value. The same notation is applied for G2.

Assuming that the connection between the VSM and G1 is mainly inductive, the power transfer in steady state can be calculated as (see Fig. 2):

$$P_{s1} = \frac{|\vec{u}_1||\vec{u}_f|}{(L_o + L_g)\omega^*} \sin\theta_{s1} \approx \frac{|\vec{u}_1||\vec{u}_f|}{(L_o + L_g)\omega^*}\theta_{s1}, \tag{8}$$

where subscript "s" refers to the VSM and θ_{s1} is the angle difference between the VSM and G1:

$$\theta_{s1}(s) = \theta_s(s) - \theta_1(s). \tag{9}$$

The approximation assumes that θ_{s1} is small. Therefore, the coefficient K_{s1} in Fig. 3 can be calculated as:

$$K_{s1} = |\vec{u}_1^o||\vec{u}_f^o|/((L_o + L_g)\omega^*), \tag{10}$$

where the superscript "o" represents steady state.

The same approach is applied to model the connection between the G1 and G2. Indeed, the power transferred between the two generators can be expressed on the general form of:

$$P_{12} = K_{12} \cdot \sin\theta_{12} \approx K_{12} \cdot \theta_{12}, \tag{11}$$

where K_{12} is a steady-state coefficient that models the transmission line connecting G1 and G2. The approximation assumes a small phase difference θ_{12} between the two generators, defined as:

$$\theta_{12}(s) = \theta_1(s) - \theta_2(s). \tag{12}$$

The phase difference can be calculated by integrating the difference between the generators frequencies, leading to:

$$\theta_{12}(s) = \frac{\omega_1(s) - \omega_2(s)}{s} = \frac{\omega_{12}(s)}{s}. \tag{13}$$

Imposing the power balance on the two areas leads to:

$$P_{e2}(s) = -P_{12}(s), \tag{14}$$

$$P_{e1}(s) = P_{12}(s) - P_{s1}(s). \tag{15}$$

Therefore, equation (5) can be rewritten as:

$$\omega_1(s) = 1/(J_1 s + D_1) \cdot (P_{m1}(s) + P_{s1}(s) - P_{12}(s)). \tag{16}$$

The mathematical model presented in this subsection can be summarised in the schematic displayed in Fig. 3.

III. VSM Damping Strategies

The term P_d in (1) represents the damping effect of the virtual swing equation of a VSM. However, the frequency droop K_ω can also contribute to the damping of the VSM speed. The implementation of the damping term is a notable differentiating characteristic between the VSM implementations available in literature. In this paper, the implementation of the damping term is considered for two distinct objectives: i) ensuring a damped behaviour of the VSM, and ii) contributing to attenuation of power system oscillations. For this purpose the damping term is defined as the sum of two terms, as:

$$P_d(s) = P_{ds}(s) + P_{d1}(s) = D_s(s) \cdot \omega_s(s) + D_1(s) \cdot \omega_1(s). \tag{17}$$

The transfer function $D_s(s)$ is applied to the rotating speed of the VSM inertia, while $D_1(s)$ is applied to the external measured frequency. In principle, additional terms for damping of oscillations in G2 can also be added to the formulation, but this would require communications or a model-based estimation of ω_2 and will not be considered in this paper. The two terms $P_{ds}(s)$ and $P_{d1}(s)$ will be further explained in the following subsections.

This is the accepted version of a paper published in 44th Annual Conference of the IEEE Industrial Electronics Society (IECON2018)
DOI: 10.1109/IECON.2018.8591097

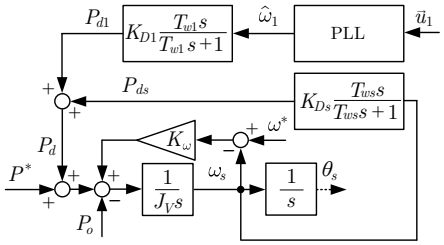

Fig. 4. VSM controller including the two damping terms.

A. Damping Strategy based on VSM speed

The term $P_{ds}(s)$ is calculated by high-pass filtering the speed of the VSM according to [23], and is implemented with the transfer function:

$$P_{ds}(s) = D_s(s) \cdot \omega_s(s) = K_{Ds}\frac{T_{ws}s}{T_{ws}s+1} \cdot \omega_s(s), \qquad (18)$$

where T_{ws} is the filter time constant and K_{Ds} is the gain of the compensator. The wash-out (high-pass) filter prevents influence on the steady-state droop characteristic associated with K_ω. The vale of T_{ws} should be large enough to influence the oscillation frequencies to be damped, but not too large because this will increase the power requirements during transients. This implementation will be labelled as "self-damping".

B. Damping Strategy based on Estimated Grid Frequency

This second damping term is based on high-pass filtering of the frequency estimated from the voltage at the VSM terminals and defined as follows:

$$P_{d1}(s) = D_1(s) \cdot \hat{\omega}_1(s) = K_{D1}\frac{T_{w1}s}{T_{w1}s+1} \cdot \hat{\omega}_1(s), \qquad (19)$$

where T_{w1} is the time-constant of the filter. The value of ω_1 is not known, so it has to be estimated ($\hat{\omega}_1$). For this purpose, a PLL has been applied in this paper. Although more advanced models can be utilized, the estimation time of the PLL is modelled with a first-order LPF, leading to:

$$\hat{\omega}_1(s) = 1/(T_{PLL}s+1) \cdot \omega_1(s), \qquad (20)$$

where T_{PLL} is the time constant of the PLL. Higher-order filters can be used to model the PLL, and this is of interest for further research. For the practical implementation, an additional low-pass filter should be added in series with the PLL to filter high-frequency noise. This damping strategy will be called "grid-damping" in the rest of the paper. For sake of clarity, the resulting control scheme for the VSM after integrating the two damping terms is summarized in Fig. 4.

IV. Numerical Results

This section presents numerical results for assessing the effect of the two damping terms on the dynamic properties the VSM and its capability for attenuating power system oscillations. A case study is first introduced based on the configuration described in section II. Thus, tuning considerations are presented on a simplified representation of the system together with a general eigenvalue stability analysis.

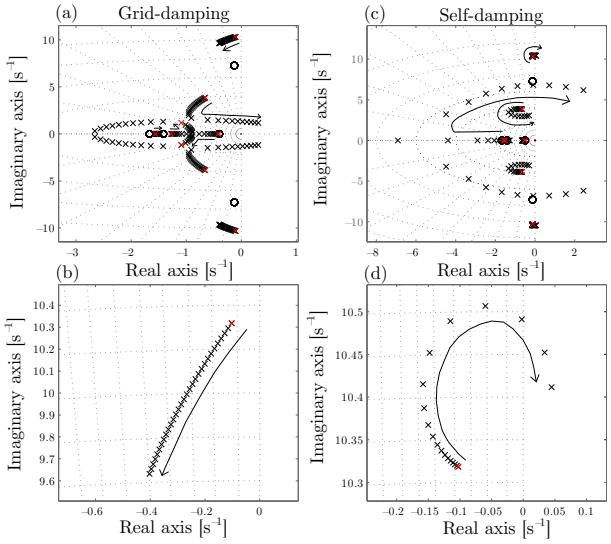

Fig. 5. Zeros and poles of the simplified system. Grid-frequency damping (a) full view and (b) zoom. VSM frequency damping (c) full view and (d) zoom.

Finally, these trends and the performance of the damping implementations are verified with time domain simulations.

A. Case Study Description

The nominal grid conditions are 400 kV RMS (phase-to-phase) and 50 Hz. The parameters of the *LCL* filter are $L_1 = 0.04$ pu ($R_1 = 0.004$ pu), $L_2 = 0.016$ pu ($R_2 = 0.001$ pu), and $C_f = 0.05$ pu ($R_d = 0$ pu). The current controller is designed with a phase margin of 60 degrees and a cross-over frequency of 250 Hz. The voltage controller is designed with a phase margin of 60 degrees and a cross-over frequency of 60 Hz. The connection between G1 and the VSM is represented as a series impedance with $L_g = 0.07$ pu and $R_g = 0.02$ pu. The parameters of the electrical model of the grid are $J_1 = 0.02$, $R_1 = 0.3$, $D_1 = 0$, $T_{g1} = 0.05$, $J_2 = 0.02$, $D_2 = 0$, $R_2 = 0.3$, and $T_{g2} = 0.05$. The value of K_{12} was set to 0.7, while K_{1s} was calculated with (10). The time constants of the wash-out filters were set to $T_{w1} = T_{ws} = 0.5$ s. The parameters of the VSM controller were set to $J_V = 0.02$, $K_\omega = 0.2$, $K_Q = 10$, and $D_Q = 50 \cdot 10^3$. For small-signal analysis, a simplified first order model of the PLL has been assumed according to [24], with a time constant of $T_{PLL} = 0.03$ s. However, a detailed discrete-time implementation of a DSOGI-PLL according to [25] has been used for time-domain simulations.

B. Eigenvalue Analysis

The dynamic performance and the stability properties of the power system when adding the damping terms are first performed by eigenvalue analysis on a simplified model. The validity of these results will be verified by detailed simulations in Section IV-C. Fig. 5 shows the eigenvalues of the system depicted in Fig. 3 when the gains for the damping terms K_{Ds} and K_{D1} are modified. In the left subplots, only the grid damping term is varied while the self damping term is disabled (i.e. $K_{Ds} = 0$). Vice versa, in the right subplots only the

This is the accepted version of a paper published in 44th Annual Conference of the IEEE Industrial Electronics Society (IECON2018)
DOI: 10.1109/IECON.2018.8591097

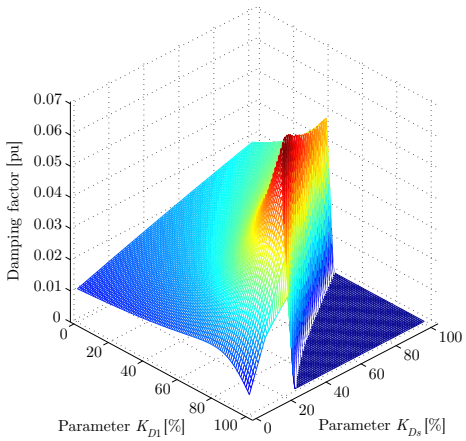

Fig. 6. Minimum damping factor of the electrical system when the parameters K_{D1} and K_{Ds} are modified.

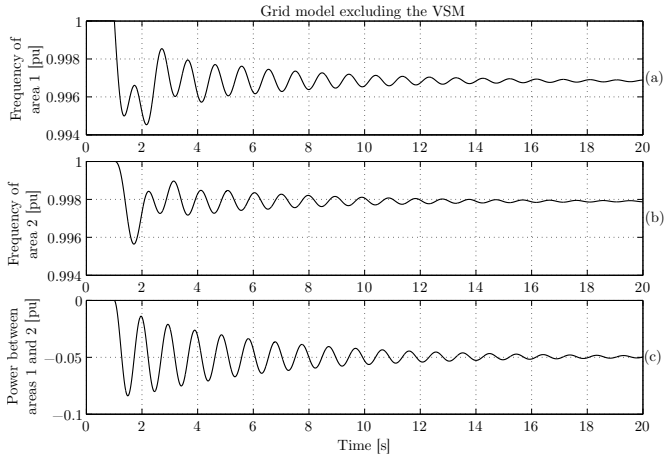

Fig. 7. Transient of the grid model when a 0.1 pu load is connected to G1 Frequency of (a) G1 and (b) G2. (c) Power transferred between areas.

self damping term is modified while the grid damping term is disabled ($K_{D1} = 0$). For the grid-damping, the resonant poles move away from the imaginary axis when K_{D1} increases. However, there is a pair of complex poles that initially move away from instability, but return towards the unstable region when the value of K_{D1} continue increasing. For the case of self-damping (to the right), the damping of the complex poles slightly improves when the gain is increased, before the poles move quickly towards the unstable region. This implies that the capability of damping the oscillations in the power system is lower than for the grid-damping.

Fig. 6 shows the lowest damping factor of all the poles included in the system model as a function of the parameters K_{D1} and K_{Ds}. Damping increases up to a point where, suddenly, another eigenvalue reaches the stability limit. The damping of the closed-loop poles related to the inter-area oscillation improves also for higher gains. However, as shown in the pole-zero analysis in Fig. 5 the low-frequency poles move towards the unstable region when the gains increase. By observing the figure, it can be seen that a combination of

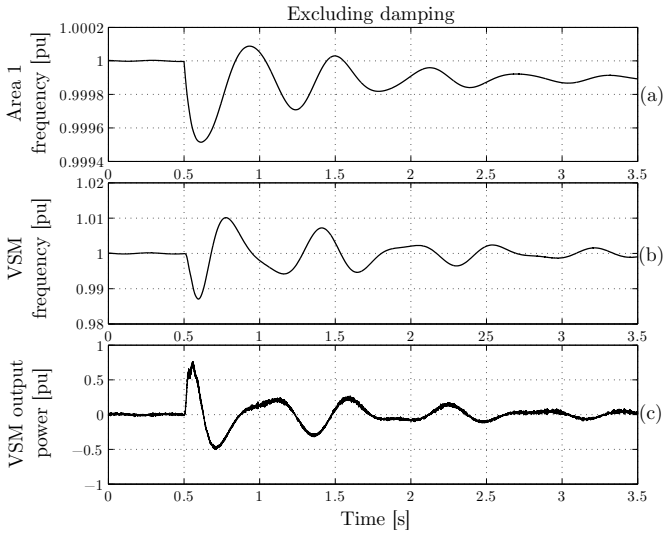

Fig. 8. Performance of the system without damping terms. (a) Grid frequency, VSM (b) frequency, (c) output power, and (d) output current.

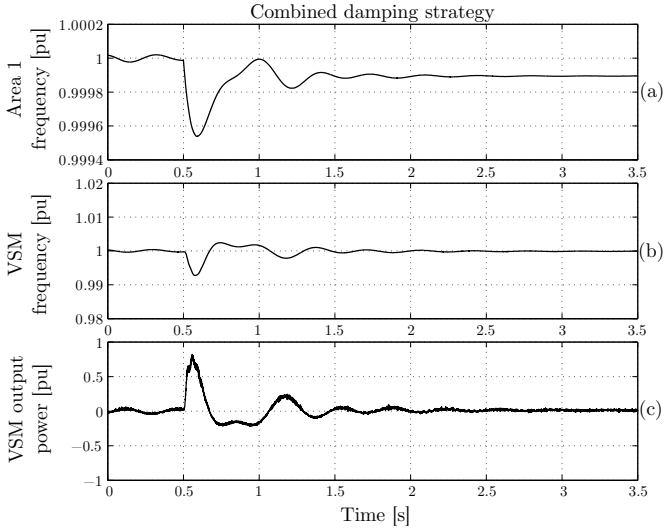

Fig. 9. Performance of the system with damping terms. (a) VSM output current, (b) frequency, (c) output power, and (d) output current.

K_{Ds} and K_{D1} provides the highest damping value and that the best results are obtained when both parameters have similar values.

C. Time Domain Simulations

A simulation model of a HVDC-VSC terminal connected to a grid is used to validate the proposed damping schemes. The model has been developed in the Matlab/Simulink environment. The sampling and switching frequencies were 5 kHz. Pulse width modulation with third harmonic injection was used. Classical decoupling equations were used for the current and voltage controllers.

1) Oscillating grid: Fig. 7 shows the performance of the electrical grid when the VSM is excluded and a 0.1 pu load is connected to G1. Initially, the frequency of both areas was constant. However, when the load was connected,

This is the accepted version of a paper published in 44th Annual Conference of the IEEE Industrial Electronics Society (IECON2018)
DOI: 10.1109/IECON.2018.8591097

the low-frequency resonance of the grid was excited. This result highlights the existence of a poorly damped oscillation between G1 and G2.

2) VSM excluding Damping: Fig. 8 shows the transient performance of the electrical system when the VSM is connected to G1. In this case, the proposed damping terms are not included in the formulation of the VSM. Although the dynamic response is still poorly damped, it can be noticed that the settling time of the oscillations has been significantly reduced compared to the case in Section IV-C1. Thus, the results, demonstrate that already the droop gain of the VSM-based control can have a non-negligible influence on the damping of the power system oscillations. However, the damping can be further improved by utilisation of the additional damping terms presented in this paper. It can also be noticed that even though the a simplified model was used to analyse the low-frequency oscillations, the oscillation frequency resulting from the simulations matches with the prediction from the eigenvalue analysis.

3) Damping of Oscillations: Fig. 9 shows the numerical results obtained when the combined damping technique is applied. Oscillations in the G1 and the VSM frequencies present in Fig. 8 have been clearly reduced. Also, the power injected from the VSM to grid is reduced compared to Fig. 8.

V. Conclusion

In this paper, two alternative implementations for damping in a VSC HVDC controlled as a VSM have been presented and assessed comparatively. The first alternative requires only the rotating speed of the VSM inertia, while the second is based on the estimated frequency of the voltage measured at converter terminals. A reference power system with two generators interconnected by a transmission line has been modelled and the effect of a 150 MVA VSM on its dynamic behaviour is examined. Eigenvalue analysis and numerical simulations demonstrated that the VSM can effectively contribute to the damping of power system oscillations. Although the damping based on estimated frequency has the strongest influence on the power system oscillations, the highest impact is obtained when both damping terms are present and optimally tuned. Both implementations in this paper adopt a first order high pass filter to isolate and identify the oscillatory mode. However, more advanced or higher order filters could be applied to further improve the performance of the system but this is considered as a topic for further research.

References

[1] H. A. Peterson and P. C. Krause, "Damping of power swings in a parallel ac and dc system," *IEEE Transactions on Power Apparatus and System*, vol. 85, no. 12, pp. 1231–1239, December 1966.

[2] R. L. Cresap and W. A. Mittelstadt, "Small-signal modulation of the pacific hvdc intertie," *IEEE Transactions on Power Apparatus and System*, vol. 95, no. 2, pp. 536–541, February 1976.

[3] A. M. Vural, "Contribution of high voltage direct current transmission systems to inter-area oscillation damping: A review," *Renewable and Sustainable Energy Reviews*, vol. 57, pp. 892–915, May 2016.

[4] L. Harnefors, N. Johansson, L. Zhang, and B. Berggren, "Interarea oscillation damping using active-power modulation of multiterminal hvdc transmissions," *IEEE Transactions on Power Systems*, vol. 29, no. 5, pp. 2529–2538, Sept. 2014.

[5] R. H. Renner and D. V. Hertem, "Ancillary services in electric power systems with hvdc grids," *IET Gener. Transm. Distrib.*, vol. 9, no. 11, pp. 1179–1185, November 2015.

[6] L. Harnefors, N. Johansson, and L. Zhang, "Impact on interarea modes of fast hvdc primary frequency control," *IEEE Transactions on Power Systems*, vol. 32, no. 2, pp. 1359–1358, March 2017.

[7] J. Zhu, C. D. Booth, G. P. Adam, A. J. Roscoe, and C. G. Bright, "Inertia emulation control strategy for vsc-hvdc transmission systems," *IEEE Trans. on Power Syst.*, vol. 28, no. 2, pp. 1227–1287, May 2013.

[8] E. Rakshani, D. Remon, A. M. Cantarellas, J. M. Garcia, and P. Rodriguez, "Modeling and sensitivity analysis of vsp based virtual inertia controller in hvdc links of interconnected power systems," *Electric Power System Research*, vol. 141, pp. 246–263, Dec. 2016.

[9] E. Rakshani, D. Remon, A. M. Cantarellas, and P. Rodriguez, "Analysis of derivative control based virtual inertia in multi-area high-voltage direct current interconnected power systems," *IET Gener. Transm. Distrib.*, vol. 10, no. 6, pp. 1458–1469, June 2016.

[10] S. D'Arco and J. A. Suul, "Virtual synchronous machines classification of implementations and analysis of equivalence to droop controllers for microgrids," in *Proc. IEEE PowerTech 2013*, June 2013, pp. 1–7.

[11] S. D'Arco, J. A. Suul, and O. B. Fosso, "A virtual synchronous machine implementation for distributed control of power converters in smartgrids," *El. Power Syst. Research*, vol. 122, pp. 180–197, 2015.

[12] L. Zhang, L. Harnefors, and H. P. Nee, "Interconnection of two very weak AC systems by VSC-HVDC links using power-synchronization control," *IEEE Trans. Pow. Sys.*, vol. 26, no. 1, pp. 344–355, Feb 2011.

[13] H. A. Alsiraji and R. El-Shatshat, "Comprehensive assessment of virtual synchronous machine based voltage source converter controllers," *IET Gen. Trans. Dist.*, vol. 11, no. 7, pp. 1762–1769, 2017.

[14] H. Zhao, Q. Yang, and H. Zeng, "Multi-loop virtual synchronous generator control of inverter-based dgs under microgrid dynamics," *IET Gen. Trans. Dist.*, vol. 11, no. 3, pp. 795–803, 2017.

[15] T. Shintai, Y. Miura, and T. Ise, "Reactive power control for load sharing with virtual synchronous generator control," in *Power Electronics and Motion Control Conference (IPEMC), 2012 7th International*, vol. 2. IEEE, 2012, pp. 846–853.

[16] K.-i. Sakimoto, K. Sugimoto, and Y. Shindo, "Low voltage ride through capability of a grid connected inverter based on the virtual synchronous generator," in *Power Electronics and Drive Systems (PEDS), 2013 IEEE 10th International Conference on*. IEEE, 2013, pp. 1066–1071.

[17] S. Sakaeda, M. Asano, S. Sugimoto, S. Verma, R. Uda, and K. Kuroda, "Studies on stabilizing a massive pv penetrated power system using vsg," in *Innovative Smart Grid Technologies Conference Europe (ISGT-Europe), 2017 IEEE PES*. IEEE, 2017, pp. 1–6.

[18] J. Roldan-Perez, A. Rodríguez-Cabero, and M. Prodanovic, "Harmonic virtual impedance design for a synchronverter-based battery interface converter," in *Renewable Energy Research and Applications (ICRERA), 2017 IEEE 6th International Conference on*. IEEE, 2017, pp. 774–779.

[19] M. Torres, L. Lopes, L. Morán, and J. Espinoza, "Self-tuning virtual synchronous machine: A control strategy for energy storage systems to support dynamic frequency control," *IEEE Transactions on Energy Conversion*, vol. 29, no. 4, pp. 833–840, Dec 2014.

[20] Y. Hirase, K. Sugimoto, K. Sakimoto, and T. Ise, "Analysis of resonance in microgrids and effects of system frequency stabilization using a virtual synchronous generator," *IEEE Journal of Emerging and Selected Topics in Power Electronics*, vol. 4, no. 4, pp. 1287–1298, Dec. 2016.

[21] J. Alipoor, Y. Miura, and T. Ise, "Power system stabilization using virtual synchronous generator with alternating moment of inertia," *IEEE Journal of Emerging and Selected Topics in Power Electronics*, vol. 3, no. 2, pp. 451–458, June 2015.

[22] M. Blau and G. Weiss, "Synchronverters used for damping inter-area oscillations in two-area power systems," in *International Conference on Renewable Energies and Power Quality (ICREPQ)*, March 2018.

[23] J. A. Suul, S. D'Arco, and G. Guidi, "A single-phase virtual synchronous machine for providing vehicle-to-grid serviced from electric vehicle battery chargers," in *Proceedings of the International Electric Vehicle Technology Conference Automotive Power Electronics, EVTeC APE Japan*, May 2014, pp. 1–7.

[24] H. Awad, J. Svensson, and M. Bollen, "Tuning software phase-locked loop for series-connected converters," *IEEE transactions on power delivery*, vol. 20, no. 1, pp. 300–308, 2005.

[25] S. Golestan, M. Monfared, and F. D. Freijedo, "Design-oriented study of advanced synchronous reference frame phase-locked loops," *IEEE Trans. on Power Electronics*, vol. 28, no. 2, pp. 765–778, Feb 2013.

This is the accepted version of a paper published in 44th Annual Conference of the IEEE Industrial Electronics Society (IECON2018)
DOI: 10.1109/IECON.2018.8591097